REAL-TIME GUITAR SYNTHESIS

Stefan Bilbao

Acoustics and Audio Group
University of Edinburgh
Edinburgh, UK
sbilbao@ed.ac.uk

Riccardo Russo, Craig J. Webb and Michele Ducceschi *

Department of Industrial Engineering
University of Bologna
Bologna, Italy
riccardo.russo19@unibo.it,
craigjonathan.webb@unibo.it,
michele.ducceschi@unibo.it

ABSTRACT

The synthesis of guitar tones was one of the first uses of physical modeling synthesis, and many approaches (notably digital waveguides) have been employed. The dynamics of the string under playing conditions is complex, and includes nonlinearities, both inherent to the string itself, and due to various collisions with the fretboard, frets and a stopping finger. All lead to important perceptual effects, including pitch glides, rattling against frets, and the ability to play on the harmonics. Numerical simulation of these simultaneous strong nonlinearities is challenging, but recent advances in algorithm design due to invariant energy quadratisation and scalar auxiliary variable methods allow for very efficient and provably numerically stable simulation. A new design is presented here that does not employ costly iterative methods such as the Newton-Raphson method, and for which required linear system solutions are small. As such, this method is suitable for real-time implementation. Simulation and timing results are presented.

1. INTRODUCTION

Sound synthesis based on physical models of stringed instruments is a very old topic, with its origins in the quasi-physical feedback delay model of Karplus and Strong [1, 2]. Major advances followed from the physical interpretation of the bidirectional delay-line pair or digital waveguide [3, 4] in terms of traveling waves—opening the door to physical modeling for a wide array of instrument types, including the guitar [5, 6], the subject of this paper.

More recently, increasingly sophisticated models of the guitar have seen investigation. One avenue has been pure musical acoustics research, where full three-dimensional modeling of the interaction of the guitar body with the acoustic field is incorporated [7, 8]. Another, geared towards synthesis applications, has been the investigation of interactions between the string, finger and fretboard, allowing for a great deal of gestural control and nuance in performance. Various techniques have been employed, including digital waveguides [9], modal methods [10] and time-stepping methods such as the finite difference time domain (FDTD) method [11, 12], which have their roots in very early attempts at synthesis [13]. Here, we adopt the latter approach, due to the very general flexibility of FDTD in handling multiple nonlinearities simultaneously. Such methods capture many subtle musical effects, including tapping, the rattling of strings against the frets and fretboard, and also the ability to play on string harmonics. See [14].

Such brute-force simulation methods are computationally intensive, and the move to real time is non-trivial. This expense stems from the strong collision nonlinearities, and the need for provably stable numerical methods (such as those ensuring energy conservation) for robust behaviour. These nonlinearities have been dealt with previously using iterative methods, such as Newton-Raphson, which are computationally intensive, and inherently serial. Recent algorithmic advances, based on invariant energy quadratisation (IEQ) [15, 16] and scalar auxiliary variable (SAV) [17, 18] approaches offer a means of sidestepping iterative methods entirely, and have been employed previously in order to accelerate physical modeling synthesis for strongly nonlinear instruments to the real-time threshold [19]. In particular, IEQ/SAV have seen use in modeling collisions within the context of musical acoustics [20, 21, 22]. In these studies, it was noted that computing the nonlinear collision force directly as the analytic potential energy gradient produced spurious oscillations, causing anomalous results in simulation, and various solutions have been proposed. Here, we present a variation of that in [22].

This paper can thus be viewed as a belated follow-up to a DAFx paper [11] from 2014, which outlined a full synthesis model of the finger/string/fretboard interaction—though well out of real time. Applying IEQ and SAV approaches allows for real-time performance for a full model of guitar string vibration for multiple strings, including four simultaneous nonlinearities: a) the distributed geometric nonlinearity in a string vibrating at high amplitudes; b) the interaction between a string with a smooth fretboard; c) the interaction between a string and an array of point-like obstacles (frets), and d) the interaction between the finger and string.

A complete model of transverse string vibration in a single polarization, including the various nonlinearities listed above, is described in Section 2, followed by a spatially semi-discrete form in Section 3, and a fully time-discrete algorithm in Section 4. Real-time implementation details and timing results follow in Section 5. and some numerical illustrations appear in Section 6. Some concluding remarks are offered in Section 7. Sound examples are available at the companion page [1].

2. MODEL SYSTEM

The model employed here appeared previously, with some minor alterations, in [11, 12], and will be presented in condensed form

* This work was supported by the European Research Council (ERC) under the Horizon2020 framework, grant number 950084-StG-NEMUS

Copyright: © 2024 Stefan Bilbao et al. This is an open-access article distributed under the terms of the Creative Commons Attribution 4.0 International License, which permits unrestricted use, distribution, adaptation, and reproduction in any medium, provided the original author and source are credited.

[1] https://physicalaudio.co.uk/guitar/

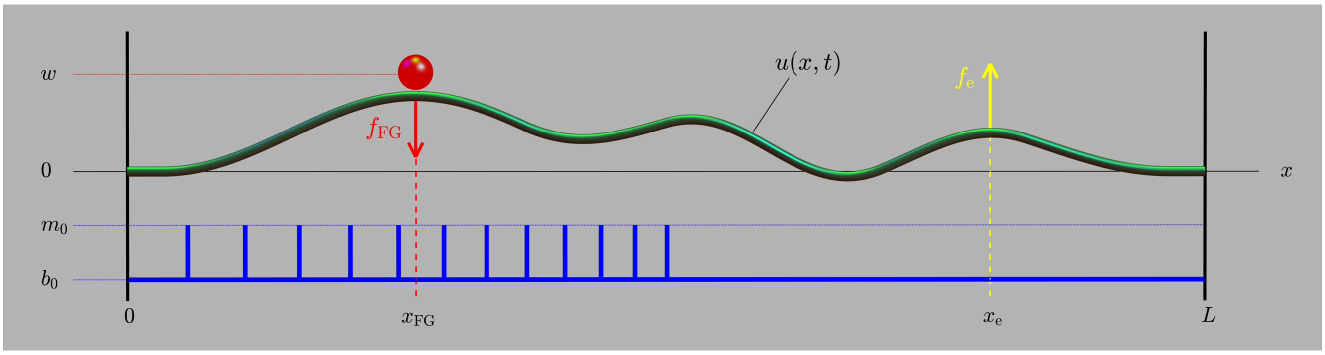

Figure 1: *Guitar model, illustrating the string (in green), the fretboard and frets (in blue), the finger (in red), and plucking excitation force (in yellow).*

here. See Figure 1. The general equation of motion is

$$\mathcal{L} = \mathcal{F}_{\mathrm{e}} + \mathcal{F}_{\mathrm{KC}} + \mathcal{F}_{\mathrm{B}} + \mathcal{F}_{\mathrm{F}} + \mathcal{F}_{\mathrm{FG}} \,. \tag{1}$$

The terms above are differential operators applied to $u = u(x,t)$, which represents the transverse displacement of a string in a single polarization (generally taken here to be perpendicular to the fretboard), and depends on spatial coordinate $x \in [0, L]$, for a string length L in m, and time t in s. Boundary conditions are assumed to be of simply supported type at the string endpoints, so that

$$u(0,t) = \partial_x^2 u(0.t) = u(L,t) = \partial_x^2 u(L,t) = 0 \,. \tag{2}$$

Output is assumed drawn directly from the string displacement at $x = x_{\mathrm{o}}$ as $y(t) = u(x_{\mathrm{o}}, t)$.

The linear free vibration of the string is encapsulated in the standard term $\mathcal{L}(u)$, defined as

$$\mathcal{L} = \rho A \partial_t^2 u - T_0 \partial_x^2 u + EI \partial_x^4 u + 2\rho A \sigma_0 \partial_t u - 2\rho A \sigma_1 \partial_t \partial_x^2 u \tag{3}$$

where ∂_t and ∂_x indicate partial differentiation with respect to t and x, respectively. The various parameters that appear here are: ρ, the mass density in kg$\cdot$ m^{-3}; $A = \pi r^2$, the string cross-sectional area in m^2 for a string of radius r m; T_0, the string tension in N; E, Young's modulus for the string, in Pa; $I = \pi r^4/4$, the moment of inertia of the string; and $\sigma_0 \geq 0$ and $\sigma_1 \geq 0$, two parameters that give frequency-dependent control over decay time—see [23] for a means of calibrating these values against 60 dB decay times.

The remaining terms in (1) are force densities, defined over the domain $x \in [0, L]$, and are presented consecutively below.

2.1. Plucking Excitation

$\mathcal{F}_{\mathrm{e}} = \mathcal{F}_{\mathrm{e}}(x,t)$ constitutes the pointwise external forcing of the string due to a single upward pluck, and may be modelled as

$$\mathcal{F}_{\mathrm{e}} = \delta(x - x_{\mathrm{e}}) f_{\mathrm{e}}(t) \,. \tag{4}$$

Here, $\delta(x - x_{\mathrm{e}})$ is a Dirac delta function selecting the plucking location $x = x_{\mathrm{e}}$, and $f_{\mathrm{e}}(t)$ is a parameterized function of the form

$$f_{\mathrm{e}}(t) = \begin{cases} f_{\mathrm{amp}} \sin^2\left(\frac{\pi(t-t_{\mathrm{e}})}{2\Delta}\right) & \text{when} \quad t_{\mathrm{e}} \leq t \leq t_{\mathrm{e}} + \Delta \\ 0 & \text{otherwise} \end{cases} \tag{5}$$

where here, f_{amp} is a maximum amplitude in N, t_{e} is the start time of the pulse in s, and Δ is the duration in s.

2.2. Geometric Nonlinearity

There are many possible models of geometric nonlinearity in strings [24]—most important here is the pitch glide effect, audible in guitar plucks at high amplitudes. This is most easily modeled through the simple Kirchhoff-Carrier model [25, 26], for which the additional force density $\mathcal{F}_{\mathrm{KC}}$ is defined as

$$\mathcal{F}_{\mathrm{KC}} = \frac{EA}{2L}\left(\int_0^L (\partial_x u)^2 \, dx\right) \partial_x^2 u \,. \tag{6}$$

The Kirchhoff-Carrier model has been used extensively in sound synthesis algorithms—see, e.g., [27, 23].

2.3. Fretboard Interaction

The fretboard (in the absence of frets) is modeled as a smooth function $b(x)$, with $b(x) \leq 0$ (so that the fretboard lies below the rest position of the string). In the simplest case, one may simply take $b(x) = b_0$, for a constant offset. The collision force density may be modelled through a penalty potential as

$$\mathcal{F}_{\mathrm{B}} = K_{\mathrm{B}} [b - u]_+^{\alpha_{\mathrm{B}}} \tag{7}$$

where $[\cdot]_+$ indicates the "positive part of," so $[\eta]_+ = (\eta + |\eta|)/2$. Here, $K_{\mathrm{B}} \geq 0$ is the fretboard stiffness, and $\alpha_{\mathrm{B}} \geq 1$ is the nonlinearity exponent. This collision force density is active only when the string is in contact with the barrier, and is otherwise zero. We employ a simple Hertzian model of contact, in line with models used in, e.g., piano hammer modelling [28], and in other models of string-barrier interaction [29, 30].

2.4. Fret Interaction

Assume that there are M frets, located at coordinates $x = x_1, \ldots, x_M$. (M is normally between 19 and 24 for standard guitars.) Interactions of the string with the frets is assumed to occur at their tips located at vertical height m_0—again with $m_0 \leq 0$, so that the rest position of the string lies above the fret tip. In addition, $m_0 \geq b(x_q)$, $q = 1, \ldots, M$, so that the frets themselves protrude from the fretboard. The resulting force density is

$$\mathcal{F}_{\mathrm{F}} = \sum_{q=1}^{M} K_{\mathrm{F}} [m_0 - u(x_q, t)]_+^{\alpha_{\mathrm{F}}} \delta(x - x_q) \,. \tag{8}$$

As in the case of the barrier, $K_{\mathrm{F}} \geq 0$ is the fret stiffness, and $\alpha_{\mathrm{F}} \geq 1$ is the nonlinearity exponent. The eventual algorithm design is insensitive to the placement of frets—for standard semitone tuning, frets should be located at coordinates $x_q = L\left(1 - 2^{-q/12}\right)$.

2.5. Finger Interaction

The finger interaction must also be modelled as a collision, but in this case has its own dynamics to account for, as well as external forcing. The finger, of mass M_{FG} in kg is assumed to act at location $x = x_{\mathrm{FG}}$. It is defined by

$$\mathcal{F}_{\mathrm{FG}} = -f_{\mathrm{FG}}\delta(x - x_{\mathrm{FG}}) \quad f_{\mathrm{FG}} = K_{\mathrm{FG}}[u(x_{\mathrm{FG}}, t) - w(t)]_+^{\alpha_{\mathrm{FG}}} . \tag{9}$$

Here, $w(t)$ is the vertical displacement of the finger—its dynamics are governed by

$$M_{\mathrm{FG}}\ddot{w} = f_{\mathrm{FG}} + f_{\mathrm{e,FG}} , \tag{10}$$

where dots indicate ordinary time differentiation. Here, $f_{\mathrm{e,FG}}(t)$ is an externally-supplied driving force, employed in order to trap the string against the fretboard and frets. (Though we assume x_{FG} to be constant in this paper, it will ultimately be allowed to vary over time, in order to effect pitch changes.)

2.6. Energy Balance

The governing equation (1), accompanied by the definitions of the various force densities in Sections 2.1 to 2.5, satisfies an energy balance of the following form:

$$\dot{H} + Q = P . \tag{11}$$

Here, H is the total stored energy in the system in J, Q and P are the power loss and supplied power, respectively, in W. Furthermore, the stored energy may be decomposed into components representing the various storage mechanisms:

$$H = T_{\mathrm{L}} + V_{\mathrm{L}} + V_{\mathrm{KC}} + V_{\mathrm{B}} + V_{\mathrm{F}} + T_{\mathrm{FG}} + V_{\mathrm{FG}} , \tag{12}$$

where components T and V indicate kinetic and potential energy, respectively. The constituent energy components and power terms are defined as follows:

$$\begin{aligned}
T_{\mathrm{L}} &= \frac{\rho A}{2}\int_0^L (\partial_t u)^2\, dx && \text{(13a)}\\
V_{\mathrm{L}} &= \frac{T_0}{2}\int_0^L (\partial_x u)^2\, dx + \frac{EI}{2}\int_0^L \left(\partial_x^2 u\right)^2 dx && \text{(13b)}\\
V_{\mathrm{KC}} &= \frac{EA}{8L}\left(\int_0^L (\partial_x u)^2\, dx\right)^2 && \text{(13c)}\\
V_{\mathrm{B}} &= \frac{K_{\mathrm{B}}}{\alpha_{\mathrm{B}} + 1}\int_0^L [b - u]_+^{\alpha_{\mathrm{B}}+1} dx && \text{(13d)}\\
V_{\mathrm{F}} &= \frac{K_{\mathrm{F}}}{\alpha_{\mathrm{F}} + 1}\sum_{q=1}^{M}[m_0 - u(x_q, t)]_+^{\alpha_{\mathrm{F}}+1} && \text{(13e)}\\
T_{\mathrm{FG}} &= \tfrac{M_{\mathrm{FG}}}{2}\dot{w}^2 && \text{(13f)}\\
V_{\mathrm{FG}} &= \tfrac{K_{\mathrm{FG}}}{\alpha_{\mathrm{FG}}+1}[u(x_{\mathrm{FG}}, t) - w]_+^{\alpha_{\mathrm{FG}}+1} && \text{(13g)}\\
Q &= 2\rho A\left(\int_0^L \sigma_0\left(\partial_t u\right)^2 + \sigma_1\left(\partial_t\partial_x u\right)^2 dx\right) && \text{(13h)}\\
P &= f_e\partial_t u(x_{\mathrm{e}}, t) + f_{\mathrm{e,FG}}\dot{w} . && \text{(13i)}
\end{aligned}$$

Note that $H \geq 0$ and $Q \geq 0$, implying that the system is dissipative in the absence of external forcing, or that $H(0) \geq H(t) \geq 0$.

3. SEMI-DISCRETE FORM

It is useful, as an intermediate step, to perform a spatial semi-discretisation of the system defined in the previous section. Suppose that the domain $[0, L]$ has been discretised with a grid spacing h, for integer $N = L/h$. Under supported boundary conditions in (2), a semi-discrete approximation to $u(x, t)$ may then be written as the $(N-1) \times 1$ column vector $\mathbf{u}(t)$, where

$$\mathbf{u} = [u_1, \ldots, u_{N-1}]^T , \tag{14}$$

where ^{T} indicates transposition. In the vectorised setting, the second spatial derivative ∂_x^2 may be approximated by the $(N-1) \times (N-1)$ negative-definite matrix $\mathbf{D}$, which is of the form

$$\mathbf{D} = \frac{1}{h^2}\begin{bmatrix} \text{-2} & 1 & & & \\ 1 & \text{-2} & 1 & & \\ & \ddots & \ddots & \ddots & \\ & & 1 & \text{-2} & 1 \\ & & & 1 & \text{-2} \end{bmatrix} .$$

Consider a Dirac delta function selecting the location $x = x_{\mathrm{c}}$. It may be approximated as

$$\delta(x - x_{\mathrm{c}}) \quad \rightarrow \quad \frac{1}{h}\mathbf{j}^{(x_{\mathrm{c}})} , \tag{15}$$

where $\mathbf{j}^{(x_{\mathrm{c}})}$ is an $(N-1) \times 1$ column vector. It may be constructed by a variety of means using, perhaps, Lagrange interpolation. In general, it will be sparse and must satisfy the first moment condition [31], or that $\mathbf{1}^T\mathbf{j}^{(x_{\mathrm{c}})} = 1$, where $\mathbf{1}$ is an $(N-1) \times 1$ vector consisting of ones (mirroring the property of the delta function that it integrates to unity). See [23]. Such a representation here can be used directly in order to simulate a pointwise forcing (as in (4), (8) or (9)), or as an interpolant, as in (8) or (9), so that

$$u(x_{\mathrm{c}}, t) \rightarrow \left(\mathbf{j}^{(x_{\mathrm{c}})}\right)^T \mathbf{u}(t) . \tag{16}$$

The object here is to arrive at a semi-discrete form of (1):

$$\mathcal{L}^{(\mathrm{s})} = \mathcal{F}_{\mathrm{e}}^{(\mathrm{s})} + \mathcal{F}_{\mathrm{KC}}^{(\mathrm{s})} + \mathcal{F}_{\mathrm{B}}^{(\mathrm{s})} + \mathcal{F}_{\mathrm{F}}^{(\mathrm{s})} - \mathcal{F}_{\mathrm{FG}}^{(\mathrm{s})} . \tag{17}$$

Distinct approaches to semi-discretisation will be taken for the different components of the model, grouped into categories as below.

3.1. Linear Operator and Excitation

The linear operator (3) may be semi-discretised immediately as

$$\mathcal{L}^{(\mathrm{s})} = \rho A\ddot{\mathbf{u}} - T_0\mathbf{D}\mathbf{u} + EI\mathbf{D}^2\mathbf{u} + 2\rho A\sigma_0\dot{\mathbf{u}} - 2\rho A\sigma_1\mathbf{D}\dot{\mathbf{u}} . \tag{18}$$

Using an approximation to a delta function as in (15), centered at x_{e}, the excitation force density (4) may be semi-discretised as

$$\mathcal{F}_{\mathrm{e}}^{(\mathrm{s})} = \frac{1}{h}\mathbf{j}^{(x_{\mathrm{e}})}f_{\mathrm{e}}(t) . \tag{19}$$

3.2. Geometric Nonlinearity

For the geometric nonlinearity, with force density as defined in (6), a semi-discrete form follows, using summation by parts, as

$$\mathcal{F}_{\mathrm{KC}}^{(\mathrm{s})} = -\frac{EAh}{2L}\left(\mathbf{u}^T\mathbf{D}\mathbf{u}\right)\mathbf{D}\mathbf{u} . \tag{20}$$

3.3. Fretboard and Frets

For the fretboard and frets, a different approach is taken here, following the SAV methodology. Here, beginning from a semi-discrete potential energy term $V_*^{(\mathrm{s})}(\mathbf{u})$, one may write

$$V_*^{(\mathrm{s})} = \tfrac{1}{2}\psi_*^2\,, \tag{21}$$

where here, ψ is a scalar auxiliary variable—the key here is that the potential energy contribution has been quadratised. At this point, semi-discrete force densities follow as

$$\mathcal{F}_*^{(\mathrm{s})} = -\tfrac{1}{h}\nabla_{\mathbf{u}} V_*^{(\mathrm{s})} = -\tfrac{1}{h}\psi_* \underbrace{\nabla_{\mathbf{u}}\psi_*}_{\mathbf{g}}\,, \tag{22}$$

where $\nabla_{\mathbf{u}}$ is a gradient with respect to the dependent variable $\mathbf{u}$. ψ becomes a new state variable, to be updated in an eventual discrete-time implementation. To this end, note that one may write

$$\dot{\psi}_* = \left(\nabla_{\mathbf{u}}\psi_*\right)^T \dot{\mathbf{u}} = \mathbf{g}_*^T\dot{\mathbf{u}}\,. \tag{23}$$

The relevant semi-discrete potential energy terms, corresponding to the fretboard and frets are:

$$\begin{aligned} V_{\mathrm{B}}^{(\mathrm{s})} &= \tfrac{K_{\mathrm{B}}h}{\alpha_{\mathrm{B}}+1}\mathbf{1}^T[\mathbf{b}-\mathbf{u}]_+^{\alpha_{\mathrm{B}}+1} & \text{(24a)}\\ V_{\mathrm{F}}^{(\mathrm{s})} &= \frac{K_{\mathrm{F}}}{\alpha_{\mathrm{F}}+1}\sum_{q=1}^{M}\left[m_0-\left(\mathbf{j}^{(x_q)}\right)^T\mathbf{u}\right]_+^{\alpha_{\mathrm{F}}+1}\,. & \text{(24b)}\end{aligned}$$

Here, $\mathbf{b} = [b_1, \ldots, b_{N-1}]^T$ is the fretboard profile sampled at the $N-1$ interior grid locations.

3.4. Finger

The case of the finger is similar to that of the frets and fretboard outlined above, but now the potential energy must include contributions from both the string and finger. Now, one may write

$$V_{\mathrm{FG}}^{(\mathrm{s})} = \frac{K_{\mathrm{FG}}}{\alpha_{\mathrm{FG}}+1}\left[\left(\mathbf{j}^{(x_{\mathbf{FG}})}\right)^T\mathbf{u}-w\right]_+^{\alpha_{\mathrm{FG}}+1} = \frac{1}{2}\psi_{\mathrm{FG}}^2 \tag{25}$$

and thus

$$\mathcal{F}_{\mathrm{FG}}^{(\mathrm{s})} = -\tfrac{1}{h}\psi_{\mathrm{FG}}\underbrace{\nabla_{\mathbf{u}}\psi_{\mathrm{FG}}}_{\mathbf{g}_{\mathrm{FG}}} \quad \text{and} \quad f_{\mathrm{FG}}^{(\mathrm{s})} = -\psi_{\mathrm{FG}}\underbrace{\frac{\partial\psi_{\mathrm{FG}}}{\partial w}}_{g'_{\mathrm{FG}}}\,. \tag{26}$$

The defining equation for w remains as in (10). It also follows that

$$\dot{\psi}_{\mathrm{FG}} = \mathbf{g}_{\mathrm{FG}}^T\dot{\mathbf{u}} + g'_{\mathrm{FG}}\dot{w}\,. \tag{27}$$

The computation of $\mathbf{g}_*$ and g'_{FG} needs to be handled carefully—see Section 4.7 for details.

3.5. Energy Balance

An energy balance in the semi-discrete case is of the form of (11):

$$\dot{H}^{(\mathrm{s})} + Q^{(\mathrm{s})} = P^{(\mathrm{s})}\,, \tag{28}$$

where $H^{(\mathrm{s})}$ has the same decomposition as in the continuous case in (12). For the linear system,

$$T_{\mathrm{L}}^{(\mathrm{s})} = \frac{\rho A h}{2}||\dot{\mathbf{u}}||^2 \quad V_{\mathrm{L}}^{(\mathrm{s})} = -\frac{T_0 h}{2}\mathbf{u}^T\mathbf{D}\mathbf{u} + \frac{EIh}{2}\mathbf{u}^T\mathbf{D}^2\mathbf{u} \tag{29}$$

where for a vector $\mathbf{f}$, $||\mathbf{f}||^2 = \mathbf{f}^T\mathbf{f}$. For the nonlinearities,

$$V_{\mathrm{KC}}^{(\mathrm{s})} = \frac{EAh^2}{8L}\left(\mathbf{u}^T\mathbf{D}\mathbf{u}\right)^2 \quad V_{\mathrm{B,F,FG}}^{(\mathrm{s})} = \frac{1}{2}\psi_{\mathrm{B,F,FG}}^2\,. \tag{30}$$

The kinetic energy for the finger, from (13f) remains unchanged under discretisation, and the loss and power terms become

$$\begin{aligned} Q^{(\mathrm{s})} &= 2\rho A h\left(\sigma_0||\dot{\mathbf{u}}||^2 - \sigma_1\dot{\mathbf{u}}^T\mathbf{D}\dot{\mathbf{u}}\right) & \text{(31a)}\\ P^{(\mathrm{s})} &= f_e\left(\mathbf{j}^{(x_{\mathrm{e}})}\right)^T\dot{\mathbf{u}} + f_{\mathrm{FG}}^{(\mathrm{ext})}\dot{w}\,. & \text{(31b)}\end{aligned}$$

The non-negativity property of $H^{(\mathrm{s})}$ and $Q^{(\mathrm{s})}$ persists in the semi-discrete case (note that $\mathbf{D}$ is negative definite by construction).

4. FULLY DISCRETE FORM

First define a time step $k = 1/f_{\mathrm{s}}$ in terms of a specified audio sample rate f_s in Hz. The $(N-1)\times 1$ vector $\mathbf{u}^n$ represents an approximation to $\mathbf{u}(t)$ at $t = nk$, for integer n. The excitation force signals $f_{\mathrm{e}}(t)$ and $f_{\mathrm{FG}}(t)$ may be sampled as f_{e}^n and f_{FG}^n, respectively. For auxiliary variables $\psi_*(t)$, as defined in (21), an interleaved approximation $\psi_*^{n+1/2}$ is employed, representing an approximation to $\psi_*(t)$ at $t = (n+1/2)k$ for integer n.

Basic shifts e_+ and e_-, applied to a time series ζ^ν, where ν is either integer, or half-integer, are defined as

$$e_+\zeta^\nu = \zeta^{\nu+1} \qquad e_-\zeta^\nu = \zeta^{\nu-1}\,. \tag{32}$$

Forward, backward and centered difference approximations to a first time derivative follow as

$$D_\pm = \pm\tfrac{1}{k}\left(e_\pm - 1\right) \quad D_\circ = \tfrac{1}{2k}\left(e_+ - e_-\right) \tag{33}$$

and averaging operators $M_\pm$ and $M_\circ$ as

$$M_\pm = \tfrac{1}{2}\left(1 + e_\pm\right) \qquad M_\circ = \tfrac{1}{2}\left(e_+ + e_-\right)\,. \tag{34}$$

An approximation to a second time derivative follows as

$$D_2 = D_+D_- = \tfrac{1}{k^2}\left(e_+ - 2 + e_-\right)\,. \tag{35}$$

As in the semi-discrete case, we proceed through the various components of the full model.

4.1. Linear Operator and Excitation

The linear semi-discrete operator defined in (18) may be discretised as follows

$$\begin{aligned} \mathcal{L}^{(\mathrm{d}),n} = {} & \rho A D_2\mathbf{u}^n - T_0\mathbf{D}\mathbf{u}^n + EI\mathbf{D}^2\mathbf{u}^n \\ & + 2\rho A\sigma_0 D_\circ\mathbf{u}^n - 2\rho A\sigma_1 D_-\mathbf{D}\mathbf{u}^n\,. \end{aligned} \tag{36}$$

This is the standard “explicit" discretisation of the linear stiff string [23]. The semi-discrete form of the excitation force density from (19) remains the same, under the replacement of $f_{\mathrm{e}}(t)$ by f_{e}^n.

4.2. Geometric Nonlinearity

Following early work on energy-conserving numerical methods for the Kirchhoff-Carrier string [32], the fully discrete form of the force density is chosen to be

$$\mathcal{F}_{\mathrm{KC}}^{(\mathrm{d}),n} = -\frac{EAh}{2L}\left((\mathbf{u}^n)^T\mathbf{D}M_\circ\mathbf{u}^n\right)\mathbf{D}\mathbf{u}^n\,. \tag{37}$$

Note the appearance of the additional time-averaging operation $M_\circ$, as defined in (34). A scalar auxiliary variable is not necessary in the discretisation of this nonlinearity.

4.3. Collisions: Fretboard and Frets

For the fretboard and frets, one may begin from the semi-discrete forms in (22) and (23), which may be discretized [18] as

$$\mathcal{F}_*^{(\mathrm{d}),n} = -\tfrac{1}{h}\left(M_-\psi_*^{n+1/2}\right)\mathbf{g}_*^n \tag{38a}$$

$$D_-\psi_*^{n+1/2} = \left(\mathbf{g}_*^n\right)^T D_\circ \mathbf{u}^n\,. \tag{38b}$$

4.4. Collisions: Finger

Finally, the dynamics of the finger are discretised as

$$M_{\mathrm{FG}} D_2 w^n = f_{\mathrm{FG}}^{(\mathrm{d}),n} + f_{\mathrm{e,FG}}^n \tag{39}$$

where $f_{\mathrm{e,FG}}^n$ is sampled from $f_{\mathrm{e,FG}}(t)$. The force density and force may be written as

$$\mathcal{F}_{\mathrm{FG}}^{(\mathrm{d}),n} = -\tfrac{1}{h}\left(M_-\psi_{\mathrm{FG}}^{n+1/2}\right)\mathbf{g}_{\mathrm{FG}}^n \quad f_{\mathrm{FG}}^{(\mathrm{d}),n} = -\left(M_-\psi_{\mathrm{FG}}\right) g_{\mathrm{FG}}^{\prime,n}\,. \tag{40}$$

It also follows that

$$D_-\psi_{\mathrm{FG}}^{n+1/2} = \left(\mathbf{g}_{\mathrm{FG}}^n\right)^T D_\circ \mathbf{u}^n + g_{\mathrm{FG}}^{\prime,n} D_\circ w^n\,. \tag{41}$$

4.5. Energy Balance and Stability Condition

A discrete-time energy balance follows from the scheme above as

$$D_- H^{(\mathrm{d})} + Q^{(\mathrm{d})} = P^{(\mathrm{d})}\,, \tag{42}$$

where the decomposition of $H^{(\mathrm{d})} = H^{(\mathrm{d}),n+1/2}$ is as in the continuous and semi-discrete cases, with all terms now assumed defined at time step $n+1/2$. For the linear system,

$$T_{\mathrm{L}}^{(\mathrm{d})} = \tfrac{\rho A h}{2}(D_-\mathbf{u}^{n+1})^T\left(\mathbf{I}_{N-1} + \sigma_1 k \mathbf{D}\right) D_-\mathbf{u}^{n+1} \tag{43a}$$

$$V_{\mathrm{L}}^{(\mathrm{d})} = \tfrac{h}{2}(\mathbf{u}^n)^T\left(-T_0\mathbf{D} + EI\mathbf{D}^2\right)\mathbf{u}^{n+1}\,. \tag{43b}$$

For the nonlinearities,

$$V_{\mathrm{KC}}^{(\mathrm{d})} = \tfrac{EAh^2}{8L}\left(\left(\mathbf{u}^{n+1}\right)^T\mathbf{D}\mathbf{u}^n\right)^2 \quad V_{\mathrm{B,F,FG}}^{(\mathrm{d})} = \tfrac{1}{2}\left(\psi_{\mathrm{B,F,FG}}^{n+1/2}\right)^2. \tag{44}$$

For the finger inertia, one has

$$T_{\mathrm{FG}}^{(\mathrm{d})} = \tfrac{M_{\mathrm{FG}}}{2}(D_- w^{n+1})^2\,. \tag{45}$$

The loss and power terms, defined at time step n, become

$$Q^{(\mathrm{d})} = 2\rho A h\left(\sigma_0\|D_\circ\mathbf{u}^n\|^2 - \sigma_1(D_\circ\mathbf{u}^n)^T\mathbf{D}D_\circ\mathbf{u}^n\right) \tag{46a}$$

$$P^{(\mathrm{d})} = f_e^n\left(\mathbf{j}^{(x_\mathrm{e})}\right)^T D_\circ\mathbf{u}^n + f_{\mathrm{e,FG}}^n D_\circ w^n\,. \tag{46b}$$

For stability, note first that $Q^{(\mathrm{d})} \geq 0$. It remains to find conditions under which the stored energy $H^{(\mathrm{d})} \geq 0$. Given that the nonlinear potential energy contributions from (44) are all non-negative, all that is necessary is to find a non-negativity condition on the linear potential and kinetic energy terms, from (43). This leads, ultimately, to the bound $h \geq h_{\min}$, where

$$h_{\min}^2 = \tfrac{k}{2}\left(\tfrac{T_0 k}{\rho A} + 4\sigma_1 + \sqrt{\left(\tfrac{T_0 k}{\rho A} + 4\sigma_1\right)^2 + \tfrac{16EI}{\rho A}}\right). \tag{47}$$

This serves as a numerical stability condition for the scheme [11].

4.6. Condensed Vector-matrix Update Form

The scheme presented in the previous sections is undeniably complex—mainly because of the use of disparate discretisation approaches for different parts of the problem—all in the interest of maximizing efficiency. The key feature is that in all the updates presented, the unknown appears linearly, meaning that iterative methods such as Newton-Raphson are not needed. What is perhaps less obvious is that the algorithm is mainly explicit, with only a small (size four) linear system solution required. It is thus useful to see the ultimate form of the update.

First, define a combined state $\mathbf{z}^n = [(\mathbf{u}^n)^T, w^n]^T$, including both the string displacement and finger displacement in a single $N \times 1$ column vector. Furthermore, one may also consolidate the three scalar potentials into a single 3×1 column vector as $\mathbf{\Psi}^{n+1/2} = [\psi_{\mathrm{B}}^{n+1/2}, \psi_{\mathrm{F}}^{n+1/2}, \psi_{\mathrm{FG}}^{n+1/2}]^T$, and the two input force signals into a 2×1 vector $\mathbf{f}^n = [f_{\mathrm{e}}^n, f_{\mathrm{e,FG}}^n]^T$. Given $\mathbf{z}^n$ and $\mathbf{z}^{n-1}$, as well as $\mathbf{\Psi}^{n-1/2}$, it is possible to write the entire update as the sequence of operations

$$\mathbf{A}^n\mathbf{z}^{n+1} = \mathbf{b}^n \quad \mathbf{\Psi}^{n+1/2} = \mathbf{\Psi}^{n-1/2} + \tfrac{1}{2}\left(\mathbf{G}^n\right)^T\left(\mathbf{z}^{n+1} - \mathbf{z}^{n-1}\right). \tag{48}$$

In the primary update of $\mathbf{z}^{n+1}$, $\mathbf{A}^n$ and $\mathbf{b}^n$ are an $N \times N$ matrix and $N \times 1$ vector, respectively; both must be constructed anew at each time step. The vector $\mathbf{b}^n$ may be written as

$$\begin{aligned}\mathbf{b}^n \;=\;& \mathbf{B}\mathbf{z}^n + \mathbf{C}\mathbf{z}^{n-1} + \mathbf{E}\mathbf{f}^n \\ & -\mathbf{\Lambda}\mathbf{G}^n\mathbf{\Psi}^{n-1/2} + \tfrac{1}{4}\mathbf{\Lambda}\mathbf{G}^n(\mathbf{G}^n)^T\mathbf{z}^{n-1} - \mathbf{k}^n(\mathbf{k}^n)^T\mathbf{z}^{n-1}\,.\end{aligned} \tag{49}$$

Here, $\mathbf{B}$ and $\mathbf{C}$ are $N \times N$ constant matrices, and $\mathbf{E}$ is an $N \times 2$ constant matrix, defined by

$$\mathbf{B} = \begin{bmatrix} \frac{1}{1+\sigma_0 k}\left(2\mathbf{I}_{N-1} + \frac{T_0 k^2}{\rho A}\mathbf{D} - \frac{EIk^2}{\rho A}\mathbf{D}^2 + 2\sigma_1 k\mathbf{D}\right) & \mathbf{0} \\ \mathbf{0} & 2 \end{bmatrix} \tag{50a}$$

$$\mathbf{C} = \begin{bmatrix} \frac{1}{1+\sigma_0 k}\left((\sigma_0 k - 1)\mathbf{I}_{N-1} - 2\sigma_1 k\mathbf{D}\right) & \mathbf{0} \\ \mathbf{0} & -1 \end{bmatrix} \tag{50b}$$

$$\mathbf{E} = \begin{bmatrix} \frac{k^2}{\rho A h(1+\sigma_0 k)}\mathbf{j}_{\mathrm{e}} & \mathbf{0} \\ 0 & \frac{k^2}{M_{\mathrm{FG}}} \end{bmatrix} \tag{50c}$$

that represent the linear dynamics of the string simulation, where $\mathbf{I}_{N-1}$ is the $(N-1)\times(N-1)$ identity matrix. All are extremely sparse. The term involving the $N \times 3$ matrix $\mathbf{G}^n$ and $N \times N$ constant diagonal scaling matrix $\mathbf{\Lambda}$, defined by

$$\mathbf{G}^n = \begin{bmatrix} \mathbf{g}_{\mathrm{B}}^n & \mathbf{g}_{\mathrm{F}}^n & \mathbf{g}_{\mathrm{FG}}^n \\ 0 & 0 & g_{\mathrm{FG}}^{\prime,n} \end{bmatrix} \quad \mathbf{\Lambda} = \begin{bmatrix} \frac{k^2}{\rho A h(1+\sigma_0 k)}\mathbf{I}_{N-1} & \mathbf{0} \\ \mathbf{0} & \frac{k^2}{M_{\mathbf{FG}}} \end{bmatrix} \tag{51}$$

follow from the collision model. Notice that the same matrix $\mathbf{G}^n$ is used in the update of $\mathbf{\Psi}^{n+1/2}$, from (48). The $N \times 1$ vector $\mathbf{k}^n$ follows from the Kirchhoff-Carrier model, and is defined as

$$\mathbf{k}^n = \tfrac{k}{2}\sqrt{\tfrac{Eh}{\rho L(1+\sigma_0 k)}}\,[(\mathbf{D}\mathbf{u}^n)^T, 0]^T\,. \tag{52}$$

Finally, the matrix $\mathbf{A}$ is defined as

$$\mathbf{A} = \mathbf{I}_N + \tfrac{1}{4}\mathbf{\Lambda}\mathbf{G}^n(\mathbf{G}^n)^T + \mathbf{k}^n(\mathbf{k}^n)^T\,. \tag{53}$$

In terms of computational cost, the main nontrivial operations are the calculations of the vectors $\mathbf{g}_*$—see the next section for more details. Beyond this, all other operations are sparse. An exception is the need for a linear system solution in (48) involving the $N \times N$ matrix $\mathbf{A}^n$ in (53). But $\mathbf{A}^n$ is in the form of a low-rank (four) perturbation of the identity, and thus very efficient resolution methods such as the Woodbury identity [33] can be employed. This avoids both the computational expense of iterative methods, and of fully linearly-implicit methods, where in general one would require the resolution of a full linear system of size N, and thus is the key to real-time performance.

Audio output y^n is drawn from the string as $y^n = (\mathbf{j}^{(x_\mathrm{o})})^T\mathbf{u}^n$, where $\mathbf{j}^{(x_\mathrm{o})}$ is an interpolant selecting the location $x = x_\mathrm{o}$.

4.7. Calculation of Potential Gradients

Vectors of the form $\mathbf{g}_*^n$, which scale with the gradient of a potential, and as defined in (22), play a central role in the operation of the scheme described above. The simplest choice for computing the nonlinear potential gradients is using the analytic expressions:

$$\tilde{\mathbf{g}}_*^n = \frac{(\nabla_\mathbf{u} V_*)^n}{\sqrt{2V_*^n + \epsilon}} \quad \tilde{g}_\mathrm{FG}^{\prime,n} = \frac{(\partial V_\mathrm{FG}/\partial w)^n}{\sqrt{2V_\mathrm{FG}^n + \epsilon}} \tag{54}$$

where ϵ is a small gauge constant [18], in this case set as machine epsilon. Here, the values V_*^n are obtained by evaluating equations (24) and (25) at time step n, and the gradients take the form:

$$(\nabla_\mathbf{u} V_\mathrm{B})^n = -hK_\mathrm{B}[\mathbf{b} - \mathbf{u}^n]_+^{\alpha_\mathrm{B}} \tag{55a}$$

$$(\nabla_\mathbf{u} V_\mathrm{F})^n = -K_\mathrm{F}\left[m_0 - \mathbf{J}^\intercal\mathbf{u}^n\right]^{\alpha_\mathrm{F}} \tag{55b}$$

$$(\partial V_\mathrm{FG}/\partial w)^n = -K_\mathrm{FG}\left[\left(\mathbf{j}^{(\boldsymbol{x}_\mathbf{FG})}\right)^T\mathbf{u}^n - w^n\right]_+^{\alpha_\mathrm{FG}} \tag{55c}$$

$$(\nabla_\mathbf{u} V_\mathrm{FG})^n = -\mathbf{j}^{(\boldsymbol{x}_\mathbf{FG})}(\partial V_\mathrm{FG}/\partial w)^n \tag{55d}$$

where $\mathbf{J}$ is a $(N-1) \times M$ matrix whose columns are the fret interpolators $\mathbf{j}^{(x_q)}$.

It is known, however, that simply using the analytic values produces an anomalous behaviour of the auxiliary variable $\psi^{n-1/2}$, that a) can exhibit long-term drift [34], and b) exhibits spurious sign flipping, meaning that the resulting force may be oriented incorrectly. The solution proposed in [22] is to impose the constraint $\psi^{n+1/2} \geq 0$. This results in a quadratic equation to be solved during contact times, yielding a scaling factor for $\tilde{\mathbf{g}}_*^n$. In this work, we propose a similar method, applied here to the computation of $\tilde{\mathbf{g}}_B^n$ and $\tilde{\mathbf{g}}_F^n$ (and not to the finger, which exhibited less drift than in the case of the fretboard or frets). The technique described here is based on the constraint: $M_-\psi_*^{n+1/2} \geq 0$. In fact, from (38a), it is apparent that if $M_-\psi_*^{n+1/2}$ remains positive, the sign of the expression is determined only by $\mathbf{g}_*^n$, which is negative by definition. This ensures that the force $\mathcal{F}_*^{(s)}$ is oriented upwards. By considering equation (38b), the constraint becomes:

$$2\psi_*^{n-1/2} + \frac{1}{2}\left(\mathbf{g}_*^n\right)^T\left(\hat{\mathbf{u}}^{n+1} - \mathbf{u}^{n-1}\right) \geq 0\,. \tag{56}$$

Here, $\hat{\mathbf{u}}^{n+1}$ is the update of the system with no external forcing, and in presence of only the relevant nonlinearity (from the fretboard or frets). In this case, the Woodbury identity reduces to the Sherman-Morrison formula [35], and one has:

$$\hat{\mathbf{u}}^{n+1} = \hat{\mathbf{b}}^n - \frac{\frac{1}{4}\hat{\boldsymbol{\Lambda}}\mathbf{g}_*^n(\mathbf{g}_*^n)^\intercal\hat{\mathbf{b}}^n}{1 + \frac{1}{4}(\mathbf{g}_*^n)^\intercal\hat{\boldsymbol{\Lambda}}\mathbf{g}_*^n}\,, \tag{57}$$

with

$$\hat{\mathbf{b}}^n = \hat{\mathbf{B}}\mathbf{u}^n + \hat{\mathbf{C}}\mathbf{u}^{n-1} - \hat{\boldsymbol{\Lambda}}\mathbf{g}_*^n\psi_*^{n-1/2} + \tfrac{1}{4}\hat{\boldsymbol{\Lambda}}\mathbf{g}_*^n(\mathbf{g}_*^n)^\intercal\mathbf{u}^{n-1}\,. \tag{58}$$

Here, $\hat{\mathbf{B}}$, $\hat{\mathbf{C}}$, $\hat{\boldsymbol{\Lambda}}$ are the upper left-hand $(N-1) \times (N-1)$ blocks of (50a), (50b) and $\boldsymbol{\Lambda}$ in (51) respectively. By inserting (57) and (58) into (56) and solving for $\mathbf{g}_*^n$ one gets:

$$4\psi_*^{n-1/2} + \underbrace{(\mathbf{g}_*^n)^\intercal(\hat{\mathbf{B}}\mathbf{u}^n + \hat{\mathbf{C}}\mathbf{u}^{n-1} - \mathbf{u}^{n-1})}_{\xi^n} \geq 0\,. \tag{59}$$

Now, as in [22], let $\mathbf{g}_*^n \triangleq \gamma\tilde{\mathbf{g}}_*^n$, where γ is a scalar. Then, (59) becomes a first-order, scalar inequality in γ. The linearity of the expression guarantees a unique solution under the condition:

$$\gamma \geq -4\psi^{n-1/2}/\xi^n\,. \tag{60}$$

Equation (60) yields a scalar multiplier for $\tilde{\mathbf{g}}_*^n$, to be applied when (59) is not satisfied for $\mathbf{g}_*^n = \tilde{\mathbf{g}}_*^n$. Thus, we set γ as:

$$\gamma = \begin{cases} -\frac{4\psi^{n-1/2}}{\xi^n}, & \text{if } \xi^n \neq 0 \quad \text{and} \quad \xi^n < -4\psi^{n-1/2} \\ -\frac{\lambda 4\psi^{n-1/2}}{\xi^{n-1}}, & \text{if } \xi^n = 0 \quad \text{and} \quad \xi^{n-1} \neq 0 \\ 1, & \text{otherwise} \end{cases}\,. \tag{61}$$

While the upper condition is designed to ensure the non-negativity of $M_-\psi_*^{n+1/2}$, the purpose of the middle condition is perhaps less obvious. Here, $\xi^{n-1} = (\tilde{\mathbf{g}}_*^{n-1})^\intercal(\hat{\mathbf{B}}\mathbf{u}^n + \hat{\mathbf{C}}\mathbf{u}^{n-1} - \mathbf{u}^{n-1})$, and the condition is satisfied only at the first instants without contact. Using the gradient from the previous time-step enforces $M_-\psi^{n+1/2} = 0$, meaning that no residual energy is stored during non-contact periods. Finally, λ is a scalar multiplier that allows the condition (60) to be satisfied away from the equality. Here, it was set $\lambda = 0.5$ if $-4\psi^{n-1/2}/\xi^{n-1} < 0$ and $\lambda = 1.5$ if $-4\psi^{n-1/2}/\xi^{n-1} \geq 0$.

5. REAL-TIME IMPLEMENTATION AND TIMING RESULTS

The algorithm was prototyped initially in the Matlab environment, and then ported to offline C++ in order to gauge the CPU performance on a number of different machines. Whilst the vector-matrix form described in Section 4.6 is algebraically compact and efficient for prototyping in Matlab, for high performance C++ the sparse matrix operations are unrolled into their equivalent vector updates. The core elements of the algorithm that are performed at each time step are as follows: a) compute the linear update to the string and finger, for the terms in (49) employing the matrices $\mathbf{B}$, $\mathbf{C}$ and $\mathbf{E}$; b) compute $\mathbf{k}^n$ from (52), and the accompanying term in (49); compute the columns of $\mathbf{G}^n$ from (51) corresponding to c) the fretboard, d) the frets and e) the finger, and the accompanying term in (49); and f) perform the linear system solution required in (48), using the construction of $\mathbf{A}^n$ from (53) and the Woodbury identity, and the update of $\Psi^{n+1/2}$ from (48). Final steps of negligible computational cost are the reading the output and a pointer swap of the state vectors. With attention to the content and data arrangement in the FOR loops being used, the Clang compiler at -Ofast was able to fully vectorise all of the core updates of the algorithm without the use of manual intrinsics.

Performance testing was carried out on a model containing a single string with 20 frets on the fretboard and a single finger. The tension and radius of the string were varied to give results for a typical set of acoustic guitar strings from low E to top E tuning. Test machines were a Mac Pro with a Xeon E5 processor, a Mac mini with Apple Silicon M1 processor, and MacBook Pro with an M2 Pro. Table 1 shows the resulting computation times for simulations of 44100 timesteps.

Table 1: *Computation times for C++ over 44100 time-steps.*

String	Xeon E5	Apple M1	Apple M2 Pro
1 (low E)	0.18s	0.13s	0.11s
2	0.18s	0.13s	0.11s
3	0.15s	0.11s	0.10s
4	0.13s	0.09s	0.08s
5	0.12s	0.08s	0.06s
6 (top E)	0.09s	0.06s	0.04s

These results show that it is possible to run a 6-voice model for a full guitar simulation within the necessary bounds for a real-time instrument. Examining the CPU usage for the various elements of the time-loop computation gives a breakdown as shown in Table 2 for a low E string (the worst case in terms of compute time).

Table 2: *Computation breakdown for optimised C++ for a low E string.*

Section	Compute %
a) Linear update	2.3%
b) Kirchhoff-Carrier	1.9%
c) Fretboard	19.1%
d) Frets	7.7%
e) Finger	5.1%
f) SAV update and solver	63.9%

6. SIMULATION RESULTS

6.1. Numerical Energy Balance

The numerical energy balance (42) is easily demonstrated under unforced conditions. In order to incorporate the effects of loss, it is direct to define a total energy $E^{(\mathrm{d})}$, including stored energy $H^{(\mathrm{d})}$ and accumulated dissipated energy $Q^{(\mathrm{d})}$ as in Section 4.5, as

$$E^{(\mathrm{d}),n+1/2} = H^{(\mathrm{d}),n+1/2} + \sum_{\nu=0}^{n} kQ^{(\mathrm{d}),\nu}\,. \qquad (62)$$

This quantity should be conserved to near machine precision. See Figure 2, illustrating the time evolution of the various components of the discrete energy, as well as the relative deviation, defined as: $\Delta E^n = \frac{E^{(d),n+1/2} - E^{(d),n-1/2}}{\lfloor H^{(d),1/2} \rfloor_2}$, where the operator $\lfloor \eta \rfloor_2$ indicates the nearest power of two to η, rounding towards zero.

6.2. Audio Simulations

Figure 3 displays the spectrograms of the output signals in three different situations: a) the string is plucked with force of $f_{\mathrm{e}} = 5$N, at $x_{\mathrm{e}} = 0.8L$, and only the geometric nonlinearity is active. A pitch glide is clearly observable; b) the string is plucked as in (a), and all nonlinearities but the finger are active. The rattling of the string against the fretboard and the frets is evident at the first instants; c) all nonlinearities are active, and the string is not plucked, but the finger is excited with a constant force of $f_{\mathrm{e},FG} = 0.9$ N, the result is similar to a finger tap sound.

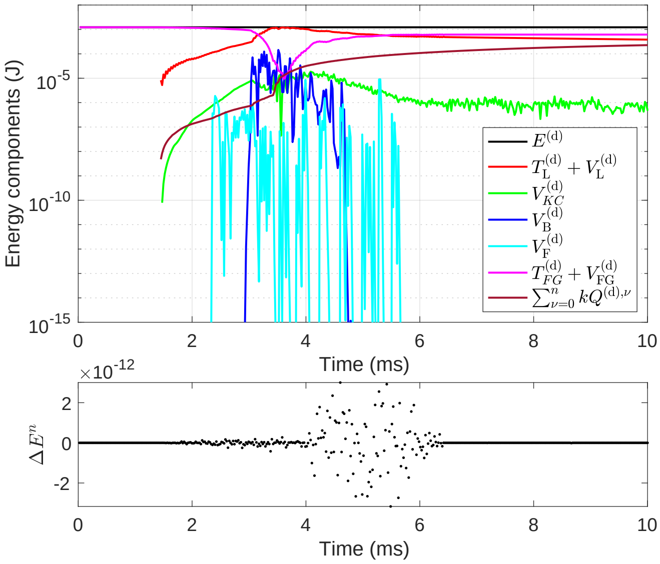

Figure 2: *Numerical energy balance. The upper panel displays the evolution of the discrete energy components over time. The string is at rest, while the finger is initially positioned above the string, with a starting velocity of* -0.7 *m/s. The second panel represents the relative energy deviation in the same situation, as defined in Section 6.1.*

7. CONCLUDING REMARKS

An efficient method for the simulation of complex dynamics of the guitar string has been presented here. In terms of efficiency, it is near to the “baseline" cost of the simulation of a string under linear conditions, while retaining the feature of an energy balance, leading to a stable algorithm. Simulation in real time for a full six-string acoustic guitar is comfortably within the capability of modest commercially-available hardware.

This good performance relies on judicious choices of discretisation strategies for the different parts of the problem—explicit methods for the linear part of the problem, coupled with specialised energy-based discretisation methods for the nonlinear components of the dynamics. Here, we have chosen to attack the four distinct nonlinearities separately, leading to a 4×4 linear system—which is not expensive. A better approach would be to consolidate all of the nonlinear dynamics into a single scalar potential, eliminating the need for any linear system solution, at the expense of less algorithmic control (and in particular the distinct approaches to the calculation of the potential gradients, as discussed in Section 4.7.

Many features have not been included here. Most important are: a) string motion in distinct polarisations, and b) the modeling of the coupling to the body and radiation. Incorporating a) is certainly possible, and would roughly double computational cost,

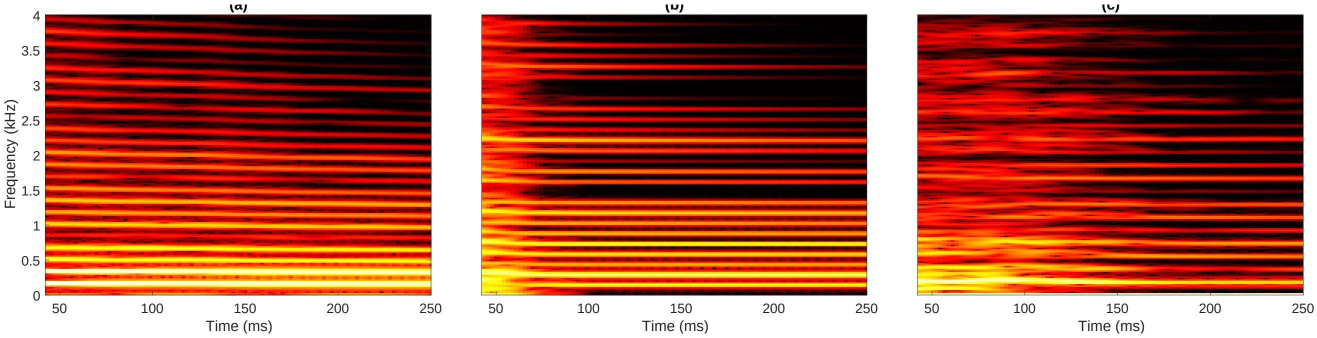

Figure 3: *Audio simulations: a) plucked string with geometric nonlinearity alone; b) plucked string with geometric, fretboard and frets nonlinearities; c) finger tap simulation. These spectrograms correspond to a guitar D string, with parameters as given in [11].*

and introduce a wider sound palette, through the angle of plucking relative to the fretboard (and the accompanying additional control complexity). Incorporating b) through a full physical model is infeasible, though such effects can be approximated through the use of measured body responses. Further work in the very near future will include plugin development, and examining the very large problem of instrument control—not addressed here.

8. REFERENCES

[1] K. Karplus and A. Strong, "Digital synthesis of plucked-string and drum timbres," *Comp. Music J.*, vol. 7, no. 2, pp. 43–55, 1983.

[2] D. Jaffe and J. O. Smith III, "Extensions of the Karplus-Strong plucked string algorithm," *Comp. Music J.*, vol. 7, no. 2, pp. 56–68, 1983.

[3] J. O. Smith III, "Efficient simulation of the reed-bore and bow-string mechanisms," in *Proc. of Int. Comp. Music Conf.*, The Hague, The Netherlands, October 1986, pp. 275–280.

[4] J. O. Smith III, "Physical modelling using digital waveguides," *Comp. Music J.*, vol. 16, no. 4, pp. 74–91, 1992.

[5] M. Karjalainen, V. Välimäki, and Z. Janosy, "Towards high-quality sound synthesis of the guitar and string instruments," in *Proc. Int. Comp. Music Conf.*, Tokyo, Japan, September 1993, pp. 56–63.

[6] M. Laurson, C. Erkut, V. Välimäki, and M. Kuuskankare, "Methods for modeling realistic playing in acoustic guitar synthesis," *Comp. Music J.*, vol. 25, no. 3, pp. 38–49, 2001.

[7] G. Derveaux, A. Chaigne, P. Joly, and E. Bécache, "Time-domain simulation of a guitar: Model and method," *J. Acoust. Soc. Am.*, vol. 114, no. 6, pp. 3368–3383, 2003.

[8] R. Bader, *Computational Mechanics of the Classical Guitar*, Springer-Verlag, Berlin Heidelberg, 2005.

[9] G. Evangelista and F. Eckerholm, "Player instrument interaction models for digital waveguide synthesis of guitar: Touch and collisions," *IEEE Trans. Audio Speech Language Proces.*, vol. 18, no. 4, pp. 822–832, 2010.

[10] V. Debut and J. Antunes, "Physical synthesis of six-string guitar plucks using the Udwadia-Kalaba modal formulation," *J. Acoust. Soc. Am.*, vol. 148, no. 2, pp. 575–587, 2020.

[11] S. Bilbao and A. Torin, "Numerical modeling of string/barrier collisions: The fretboard," in *Proc. 17th Int. Conf. Digital Audio Effects*, Erlangen, Germany, Sept. 2014.

[12] S. Bilbao and A. Torin, "Numerical modeling and sound synthesis for articulated string/fretboard interactions," *J. Audio Eng. Soc.*, vol. 63, no. 5, pp. 336–347, 2015.

[13] L. Hiller and P. Ruiz, "Synthesizing musical sounds by solving the wave equation for vibrating objects: Part I," *J. Audio Eng. Soc.*, vol. 19, no. 6, pp. 462–70, 1971.

[14] S. Bilbao, C. Desvages, M. Ducceschi, B. Hamilton, R. Harrison, A. Torin, and C. Webb, "Physical modeling, algorithms and sound synthesis: The NESS project," *Comp. Music J.*, vol. 43, no. 2/3, pp. 15–30, 2020.

[15] X. Yang and D. Han, "Linearly first- and second-order, unconditionally energy stable schemes for the phase field crystal model," *J. Comp. Phys.*, vol. 330, pp. 1116–1134, 2016.

[16] X. Yang, J. Zhao, and Q. Wang, "Numerical approximations for the molecular beam epitaxial growth model based on the invariant energy quadratization method," *J. Comp. Phys.*, vol. 333, pp. 104–127, 2017.

[17] J. Shen, J. Xu, and J. Yang, "The scalar auxiliary variable (SAV) approach for gradient flows," *J. Comp. Phys.*, vol. 353, pp. 407–416, 2018.

[18] S. Bilbao, M. Ducceschi, and F. Zama, "Explicit exactly energy-conserving methods for hamiltonian systems," *J. of Comp. Phys.*, vol. 472, pp. 111697, 2023.

[19] M. Ducceschi and S. Bilbao, "Simulation of the geometrically exact nonlinear string via energy quadratisation," *J. Sound Vib.*, vol. 534, pp. 117021, 2022.

[20] M. Ducceschi and S. Bilbao, "Real-time simulation of the struck piano string with geometrically exact nonlinearity via novel quadratic hamiltonian method," in *Proc. 10th Eur. Nonlinear Dynamics Conf.*, Lyon, France, July 2022.

[21] M. Ducceschi, S. Bilbao, S. Willemsen, and S. Serafin, "Linearly-implicit schemes for collisions in musical acoustics based on energy quadratisationa)," *J. Acoust. Soc. Am.*, vol. 149, no. 5, pp. 3502–3516, 05 2021.

[22] M. van Walstijn, V. Chatziioannou, and A. Bhanuprakash, "Implicit and explicit schemes for energy-stable simulation of string vibrations with collisions: Refinement, analysis, and comparison," *J. Sound Vib.*, vol. 569, pp. 117968, 2024.

[23] S. Bilbao, *Numerical Sound Synthesis: Finite Difference Schemes and Simulation in Musical Acoustics*, John Wiley and Sons, Chichester, UK, 2009.

[24] P. Morse and U. Ingard, *Theoretical Acoustics*, Princeton University Press, Princeton, NJ, USA, 1968.

[25] G. Kirchhoff, *Vorlesungen über Mechanik*, Tauber, Leipzig, 1883.

[26] G. F. Carrier, "On the non-linear vibration problem of the elastic string," *Q. Appl. Math.*, vol. 3, no. 2, pp. 157–165, 1945.

[27] T Tolonen, V. Välimäki, and M. Karjalainen, "Modelling of tension modulation nonlinearity in plucked strings," *IEEE Trans. Speech Audio Proces.*, vol. 8, pp. 300–310, 2000.

[28] A. Chaigne and A. Askenfelt, "Numerical simulations of struck strings. I. A physical model for a struck string using finite difference methods," *J. Acoust. Soc. Am.*, vol. 95, no. 2, pp. 1112–1118, 1994.

[29] S. Bilbao, A. Torin, and V. Chatziioannou, "Numerical modeling of collisions in musical instruments," *Acta Acustica u. Acustica*, vol. 101, no. 1, pp. 155–1731, 2015.

[30] V. Chatziioannou and M. van Walstijn, "Energy conserving schemes for the simulation of musical instrument contact dynamics," *J. Sound Vib.*, vol. 339, pp. 262–279, 2015.

[31] B. Hosseini, N. Nigam, and J. Stockie, "On regularizations of the Dirac delta distribution," *J. Comp. Phys.*, vol. 305, pp. 423–447, 2016.

[32] S. Bilbao and J. O. Smith III, "Energy conserving finite difference schemes for nonlinear strings," *Acustica*, vol. 91, pp. 299–311, 2005.

[33] M Woodbury, "Inverting modified matrices," Tech. Rep., Princeton, New Jersey, USA, 1950, Statistical Research Group, Memo. Rep. no. 42.

[34] R. Russo, S. Bilbao, and M. Ducceschi, "Scalar auxiliary variable techniques for nonlinear transverse string vibration," *IFAC-PapersOnLine*, Accepted for publication, IFAC Workshop on Lagrangian and Hamiltonian Methods for Nonlinear Control LHMNC.

[35] J. Sherman and W. J. Morrison, "Adjustment of an inverse matrix corresponding to a change in one element of a given matrix," *Ann. Math. Stat.*, vol. 21, pp. 124–127, 1950.

[36] G. Evangelista and J. O. Smith, "Structurally passive scattering element for modeling guitar pluck action," in *Proc. 13th Int. Conf. Digital Audio Effects*, Graz, Austria, Sept. 2010, pp. 10–17.